

We are IntechOpen, the world's leading publisher of Open Access books Built by scientists, for scientists

4,800

Open access books available

122,000

International authors and editors

135M

Downloads

Our authors are among the

154

Countries delivered to

TOP 1%

most cited scientists

12.2%

Contributors from top 500 universities



WEB OF SCIENCE™

Selection of our books indexed in the Book Citation Index
in Web of Science™ Core Collection (BKCI)

Interested in publishing with us?
Contact book.department@intechopen.com

Numbers displayed above are based on latest data collected.
For more information visit www.intechopen.com



Improved Inertial/Odometry/GPS Positioning of Wheeled Robots Even in GPS-Denied Environments

Eric North¹, Jacques Georgy², Umar Iqbal³, Mohammed Tarbochi⁴
and Aboelmagd Noureldin⁵

¹*Canadian Forces Aerospace and Telecommunications Engineering Support Squadron*

²*Trusted Positioning Inc.*

³*Electrical and Computer Engineering Department, Queen's University*

⁴*Electrical and Computer Engineering Department, Royal Military College*

⁵*Electrical and Computer Engineering Department, Royal Military College/Queen's
University
Canada*

1. Introduction

As described by Pacis et al (Pacis et al., 2004) the control strategy from a navigational viewpoint used in a mobile platform ranges from tele-operated to autonomous. A tele-operated platform is a platform having no on-board intelligence and whose navigation is guided in real-time by a remote human operator. An autonomous platform is one that takes its own decisions using onboard sensors and processor. According to Pacis et al (Pacis et al., 2005) for autonomous mobile robot navigation the problems that must be dealt with are localization, path planning, obstacle avoidance and map building. The focus of this work is in the localization problem.

Localization is the problem of estimating robot's pose relative to its environment from sensor observations. Localization is a necessity for successful mobile robot systems, it has been referred to as "the most fundamental problem to providing a mobile robot with autonomous capabilities" (Cox, 1991). Furthermore, as confirmed in (Pacis et al., 2004) to achieve autonomous navigation the robot must maintain an accurate knowledge of its position and orientation. Successful achievement of all other navigation tasks depends on the robot's ability to know its position and orientation accurately. According to a review by Borenstein et al (Borenstein et al., 1997) of mobile robot positioning technologies, positioning systems are divided into seven categories falling in two groups. They classified the positioning techniques as: relative position measurement and absolute position measurement. The former includes odometry and inertial navigation while the latter includes magnetic compass, active beacons, global positioning system (GPS), landmark navigation and map-based positioning.

An unprecedented surge of developments in mobile robot outdoor navigation was witnessed after the US government removed selective availability (SA) of GPS. Examples of applications

for these robots are autonomous lawnmowers and motorized wheelchairs. These devices are low-cost and are used on terrain that is not flat. GPS can be used to provide three-dimensional knowledge of the mobile robot's position. Unfortunately, GPS suffers from outages when line-of-sight is blocked between the robot and GPS satellites. These outages are caused by operating the robot in and around buildings, dense foliage and other obstructions. An inertial measurement unit (IMU), with three accelerometers and three gyroscopes, is a good choice in lieu of GPS during outages for providing a 3-D positioning solution. Since a low-cost solution is needed for certain mobile robots, a low-cost IMU based on a micro electro-mechanical system (MEMS) has to be used. However, MEMS-based inertial sensors suffer from several complex errors such as biases; moreover these errors have influential stochastic parts. Since inertial navigation systems (INS) involve integration operations using sensor readings, the subsequent errors will accumulate and cause a rapid degrade in the quality of position estimate. Odometry using wheel encoders is another type of dead reckoning that provides limited localization information, mostly two-dimensional (2-D). This information is not subject to the same magnitude of errors as the IMU, provided that the vehicle does not encounter excessive skidding or slipping. But these 2-D solutions will not be adequate if the robot often moves outside the horizontal plane.

While 2-D and 3-D solutions using sensors in a full-sized vehicle have been done in the work to-date, further research is needed in the area of 3-D localization of small wheeled mobile robots operating in large 3-D terrain. The majority of the previous work using small mobile robots shows that the terrain is flat and the paths of the robots are small (for example (Ohno et al., 2003)(Ollero et al., 1999)(Chong & Kleeman, 1997)). This work attempts to bridge the gap between full-sized vehicle navigation in 3-D and navigation of small wheeled mobile robots over large paths in uneven terrain. Furthermore, this work will provide a 3-D solution for a small wheeled mobile robot that is required to travel distances in excess of 1 km over hilly terrain.

This work aims at combining the advantages of inertial sensors and odometry while mitigating their disadvantages to provide enhanced low-cost mobile robot 3-D localization capabilities during GPS outages. This will be achieved through the use of a Kalman Filter (KF) that integrates odometry from wheel encoders, low cost MEMS-based inertial sensors and GPS in a loosely-coupled scheme. To enhance the performance and lower the cost further, the proposed technique uses a reduced inertial sensor system (RISS). To further enhance the solution during GPS outages, velocity updates computed from wheel speeds are used to reduce the drift of the estimated solution. Moreover, this work proposes the development of a predictive error model used in a KF for estimating the errors in positions, velocities and azimuth angle from RISS mechanization. The experimental results will show that this error model when combined in a KF with 3-D measurement updates of velocities using forward speed from encoders together with pitch and azimuth estimates is a good technique for greatly reducing localization errors.

The structure of the rest of this chapter is as follows: Section 2 presents the methodology used. It describes the equations used to implement the RISS mechanization and KF error-models. Section 3 is a description of the mobile robot and the setup used in the experiments. Section 4 presents the results and discussion of this work. Finally, Section 5 is the conclusion and discussion of future work.

2. Methodology

2.1 Reduced inertial sensor system

In addition to MEMS-based sensors, the concept of RISS is used in a navigation scheme for a full-sized vehicle (Iqbal et al., 2008) in order to further lower the cost of the positioning solution. The RISS used in (Iqbal et al., 2008) involves a single-axis gyroscope and two-axis accelerometer together with a built-in vehicle speed sensor to provide a 2-D navigation solution in denied GPS environments. With the assumption that the vehicle remains mostly in the horizontal plane, the vehicle's speed sensor is used with heading information obtained from the vertically-aligned gyroscope to determine the velocities along the East and North directions. Consequently, the vehicle's longitude and latitude are determined. If pitch and roll angles are needed the two accelerometers pointing towards the forward and transverse directions are used together with odometer-derived speed and a reliable gravity model to determine these angles independently of the integration filter. In (Iqbal et al., 2009), 2-D RISS/GPS integration were presented using Kalman filter (KF) for a full-sized vehicle.

In this work a low-cost navigation system using a KF to integrate MEMS-based RISS with GPS in a loosely-coupled scheme is described. The RISS used herein is 3-D: it includes a three-axis accelerometer and a single-axis gyroscope aligned with the vertical axis of the body frame of the robot together with two wheel encoders. Here accelerometers are used to calculate 3-D velocity and position while the vertical gyroscope is used to calculate the azimuth angle (i.e. the heading of the robot). Pitch and roll are calculated based on the idea presented in (Noureldin et al., 2002)(Noureldin et al., 2004) using the two horizontal accelerometers and the forward velocity obtained from wheel encoders. This constitutes the RISS mechanization.

The benefits of eliminating the other two gyroscopes in this RISS mechanization scheme are as follows: (1) further decreases in system costs and (2) improvements in positioning accuracy by employing fewer inertial sensors and thus less contribution of sensor errors towards positional errors. Of particular importance is the reduction in error in pitch and roll calculations. Whereas full mechanization of pitch and roll from gyroscopes involves integration, their calculation in RISS mechanization using accelerometers does not. This last fact decreases the portion of positional error originating from pitch and roll errors.

2.2 Coordinate transformation from local level frame (LLF) to body frame (B-F)

The local level frame (LLF) serves to represent mobile robot attitude and velocity for operation on or near the surface of the earth and is defined as an origin, x, y and z-axis. The origin coincides with the center of the sensor frame (origin of inertial sensor triad). The y-axis points to true north. The x-axis points to east. Finally, the z-axis completes the right-handed coordinate systems pointing up, perpendicular to the reference ellipsoid.

One of the important direction cosine matrices for specifying rotation between one coordinate frame to another is \mathbf{R}_b^l which transforms a vector from b -frame to LLF, a requirement during the mechanization process. \mathbf{R}_b^l is expressed in terms of yaw, pitch and roll Euler angles is defined as:

$$\mathbf{R}_b^l = \begin{bmatrix} \cos \psi \cos \theta - \sin \psi \sin \rho \sin \theta & -\sin \psi \cos \rho & \cos \psi \sin \theta + \sin \psi \sin \rho \sin \theta \\ \sin \psi \cos \theta + \cos \psi \sin \rho \sin \theta & \cos \psi \cos \rho & \sin \psi \sin \theta - \cos \psi \sin \rho \cos \theta \\ -\cos \rho \sin \theta & \sin \rho & \cos \rho \cos \theta \end{bmatrix} \quad (1)$$

2.3 Mobile robot odometry equation

The conventions and notation presented in (Chong & Kleeman, 1997) are used to create a kinematic model for the mobile robot. In this work, a simple model for mobile robot kinematics is considered. The wheels must be as thin as possible (one rolling point-of-contact between the terrain and each wheel). Also, there must not be any slipping along the longitudinal direction. There must not be any sliding along the transverse direction.

Define the instantaneous center of curvature (ICC) as a means of describing the curvilinear motion that the mobile robot makes on a plane. In a two-dimensional environment the plane that the robot travels on remains fixed for all possible positions and orientations of the mobile robot (some authors refer to the reference frame enclosed in this plane as the "global reference frame" (Chong & Kleeman, 1997)). In this work, motion of the mobile robot on possibly distinct planes for each time interval is considered. The mobile robot travels on a plane that is fixed from time $k - 1 \leq t \leq k + 1$.

$$V_{T_k} = \frac{r_R \omega_{R_k} + r_L \omega_{L_k}}{2} \quad (2)$$

where:

V_{T_k} is the velocity of the robot measured from its center and tangent to the circular path contained on a plane from time $k - 1 \leq t \leq k + 1$;

r_R is the radius of the right drive wheel;

r_L is the radius of the left drive wheel;

ω_{R_k} is the angular velocity of the right drive wheel from time $k - 1 \leq t \leq k + 1$;

ω_{L_k} is the angular velocity of the left drive wheel from time $k - 1 \leq t \leq k + 1$;

k represents discrete time epochs; and

Δt is the sampling time.

Rotational speeds of the left and right drive wheels are measured using encoders which are used to calculate the forward velocity of the robot. The forward velocity is transformed into velocities in the local frame using the equations below. Equation 2 is expressed in the mobile robot frame. In order for us to use the velocities of the robot's wheels as a measurement update we must transform these quantities to the local frame. Using the following transformation we have:

$$V_{e_k}^{odo} = V_{T_k} \cos(\rho_k) \sin(\alpha_k) \quad (3)$$

$$V_{n_k}^{odo} = V_{T_k} \cos(\rho_k) \cos(\alpha_k) \quad (4)$$

$$V_{u_k}^{odo} = V_{T_k} \sin(\rho_k) \quad (5)$$

2.4 RISS mechanization

2.4.1 Attitude equations

The equations for calculating pitch and roll from accelerometers are based on the idea presented in (Noureldin et al., 2002)(Noureldin et al., 2004). The robot acceleration derived from wheel encoder measurements is removed from the forward accelerometer measurement before computing the pitch angle. The equation for pitch ρ and neglecting acceleration in the forward direction since the robot travels at very low speeds is as follows:

$$\rho = \sin^{-1} \left(\frac{f_y - a_f}{g} \right) \approx \sin^{-1} \left(\frac{f_y}{g} \right) \quad (6)$$

Where:

f_y is the forward accelerometer reading;

g is the acceleration due to gravity; and

a_f is the forward acceleration and is derived from the forward velocity of the robot calculated from the average velocity measured by the wheel encoders from Equation 2.

The transverse accelerometer has to be compensated for the normal acceleration of the vehicle and then it is used to calculate the roll angle. The equation for roll θ :

$$\theta = -\sin^{-1} \left(\frac{f_x + V_f \omega_z}{g \cos \rho} \right) \quad (7)$$

Where:

f_x is the transversal accelerometer reading; and

ω_z is the vertical gyroscope reading.

The equation for the time-rate-of-change of yaw according to (Iqbal et al., 2009) using the previous value for V_e from RISS mechanization:

$$\dot{\psi} = \omega_z - \omega_e \sin \phi - V_e \frac{\tan \phi}{R + h} \quad (8)$$

Integrating in discrete time gives us:

$$\psi(k) = \psi(k-1) + \dot{\psi}(k) \Delta t \quad (9)$$

2.4.2 Velocity equations

There are three accelerometers that can be used to measure acceleration in the body frame of the mobile robot. Use these acceleration values to compute a velocity increment in the current time-step in order to compute an estimate for velocities. Use roll, pitch and yaw to calculate a rotation matrix \mathbf{R}_b^l from the body frame to the local frame in Equation 1. Calculate a skew-symmetric matrix ω_{ie}^l for the earth's rotation rate since the last velocity calculation. In addition, calculate the skew-symmetric matrix ω_{el}^l for the LLF change-of-orientation since last calculation.

Using \mathbf{R}_b^l from Equation 1, calculate the skew-symmetric matrix for earth rotation rate ω_{ie}^l since the last velocity calculation:

$$\omega_{ie}^l = \begin{bmatrix} 0 & -\omega_e \sin \phi & \omega_e \cos \phi \\ \omega_e \sin \phi & 0 & 0 \\ -\omega_e \cos \phi & 0 & 0 \end{bmatrix} \quad (10)$$

In addition, calculate the skew-symmetric matrix for the L-frame change of orientation ω_{el}^l since last calculation:

$$\omega_{el}^l = \begin{bmatrix} 0 & -\frac{V_e \tan \phi}{N+h} & \frac{V_e}{N+h} \\ \frac{V_e \tan \phi}{N+h} & 0 & \frac{V_n}{M+h} \\ -\frac{V_e}{N+h} & -\frac{V_n}{M+h} & 0 \end{bmatrix} \quad (11)$$

Use the following equation to provide velocity increments of the mobile robot in the body frame:

$$\Delta \vec{V}^b = \begin{bmatrix} f_x \Delta t \\ f_y \Delta t \\ f_z \Delta t \end{bmatrix} \quad (12)$$

With the three matrices \mathbf{R}_b^l , ω_{ie}^l and ω_{el}^l , the effect of gravity in the local frame in addition to the body-frame velocity increments $\Delta \vec{V}^b$ the new velocities are calculated by determining the rate-of-change for velocity increments $\Delta \vec{V}^l$ in the local frame as follows:

$$\Delta \vec{V}^l = \mathbf{R}_b^l \Delta \vec{V}^b - \left(2\omega_{ie}^l + \omega_{el}^l \right) \vec{V}^l \Delta t + \vec{g}^l \Delta t \quad (13)$$

Where $\vec{g}^l = [0 \ 0 \ -g]^T$. Integration is performed using the previous values for velocities \vec{V}^l at time $k-1$ to get \vec{V}^l at time k using $\Delta \vec{V}^l$ as follows:

$$\vec{V}^l(k) = \vec{V}^l(k-1) + 0.5 \left[\Delta \vec{V}^l(k) + \Delta \vec{V}^l(k-1) \right] \quad (14)$$

2.4.3 Position equations

The equations for altitude h , latitude ϕ and longitude λ are as follows:

$$h(k) = h(k-1) + 0.5 [V_u(k) + V_u(k-1)] \Delta t \quad (15)$$

$$\phi(k) = \phi(k-1) + 0.5 [V_n(k) + V_n(k-1)] \frac{\Delta t}{R+h} \quad (16)$$

$$\lambda(k) = \lambda(k-1) + 0.5 [V_e(k) + V_e(k-1)] \frac{\Delta t}{(R+h) \cos \phi} \quad (17)$$

It should be noted that any uncompensated bias or drift error in the accelerometer data will lead to growing errors when integrating acceleration to get velocity and again when integrating to get position. Furthermore, any uncompensated bias or drift error in the vertical gyroscope reading will lead to error growth when integrating to get yaw and again (together with velocity) to get position.

2.5 Kalman filtering

KF is the most commonly used technique for INS/GPS integration (Farrell & Barth, 1998)(Grewal et al., 2007). fig 1 shows a top-level view of the KF-based system used in this chapter for outdoor mobile robot localization. As mentioned previously, a loosely-coupled integration scheme is adopted in this chapter.

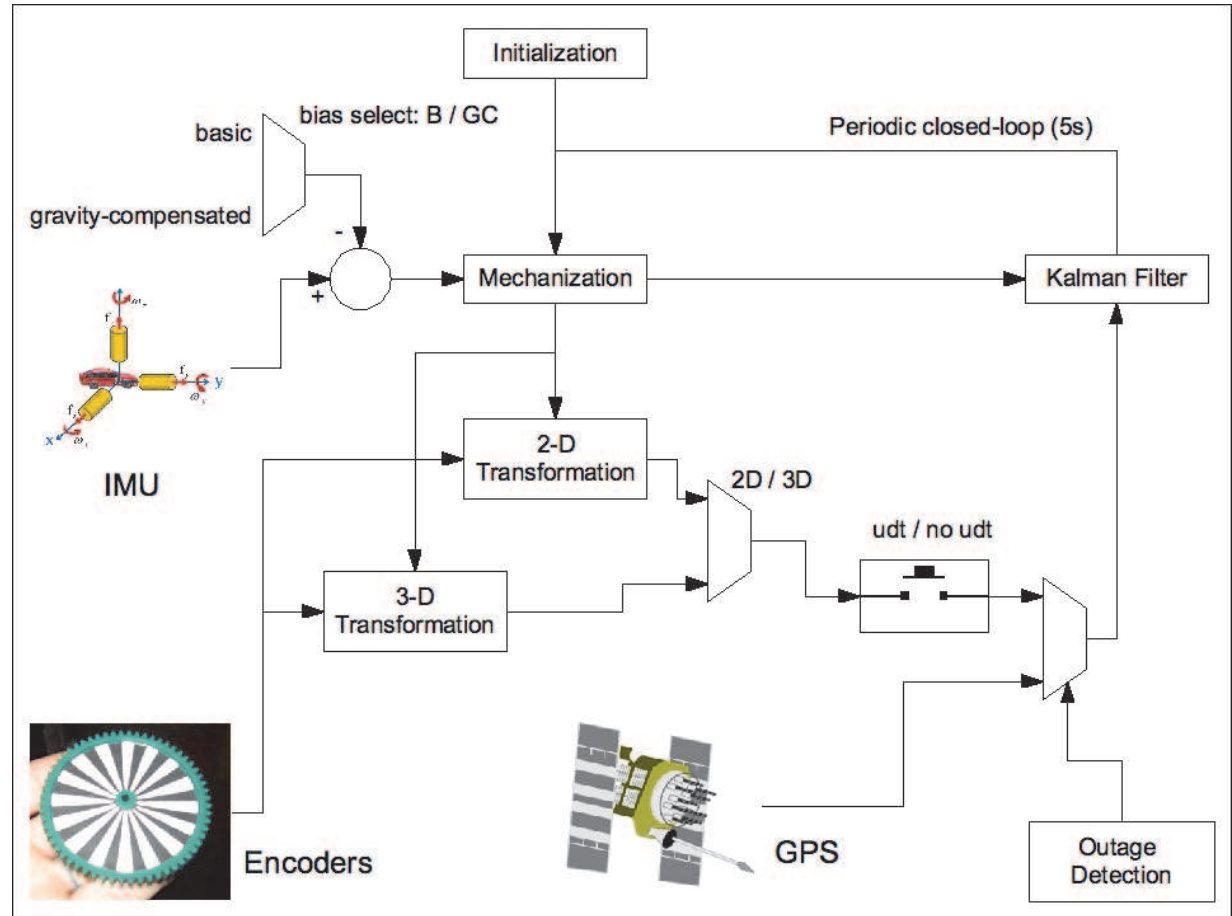


Fig. 1. An overview of the KF-based system used for outdoor mobile robot localization.

2.5.1 Error state vector

Since KF requires linearized models it estimates the error state not the navigation states themselves. The errors in the navigation states estimated by the filter are then used to correct the mechanization output and provide corrected navigation states. Leveraging the benefits of wheel encoders during GPS outages the KF presented in this section uses an error vector containing eleven states.

The linearized error-state system model used by the KF in this work is in the form:

$$\delta \dot{\vec{x}} = \mathbf{F} \delta \vec{x} + \mathbf{G} \mathbf{W}(t) \tag{18}$$

The error state vector in Equation 18 consists of position errors (for latitude, longitude and altitude), velocity errors (along East, North and vertical Up), yaw error and inertial sensor stochastic drift for the single gyroscope and three accelerometers:

$$\delta \vec{x} = [\delta \phi \quad \delta \lambda \quad \delta h \quad \delta \dot{V}_e \quad \delta \dot{V}_n \quad \delta \dot{V}_u \quad \delta \psi \quad \delta \dot{\omega}_z \quad \delta \dot{f}_x \quad \delta \dot{f}_y \quad \delta \dot{f}_z]^T \tag{19}$$

The following sections contain derivations of the equations for each error state in the model. These equations use first order terms from the Taylor series expansion of the mechanization equations.

2.5.2 Position errors

From (Noureldin et al., 2009) the position components of the mechanization equations are linearized, yielding three error equations for latitude, longitude and altitude. Neglecting higher-order terms of the Taylor Series and writing in matrix form gives:

$$\delta \dot{\mathbf{r}}^l = \begin{bmatrix} \delta \dot{\phi} \\ \delta \dot{\lambda} \\ \delta \dot{h} \end{bmatrix} = \begin{bmatrix} 0 & 0 & -\frac{V_n}{(M+h)^2} \\ \frac{V_e \tan \phi}{(N+h) \cos \phi} & 0 & -\frac{V_e}{(N+h)^2 \cos \phi} \\ 0 & 0 & 0 \end{bmatrix} \begin{bmatrix} \delta \phi \\ \delta \lambda \\ \delta h \end{bmatrix} + \begin{bmatrix} 0 & \frac{1}{M+h} & 0 \\ \frac{1}{(N+h) \cos \phi} & 0 & 0 \\ 0 & 0 & 1 \end{bmatrix} \begin{bmatrix} \delta V_e \\ \delta V_n \\ \delta V_u \end{bmatrix} \quad (20)$$

Where M and N are the respective Meridian and normal radii of the curvature of the Earth.

2.5.3 Velocity errors

The velocity components from the mechanization equations are linearized to provide velocity error equations; these equations are presented in (Noureldin et al., 2009). The velocity errors are function of errors in position, velocity, and attitude as well as accelerometer stochastic drift errors.

$$\delta \dot{\mathbf{V}}^l = \begin{bmatrix} \delta \dot{V}_e \\ \delta \dot{V}_n \\ \delta \dot{V}_u \end{bmatrix} = \begin{bmatrix} 2\omega_e V_u \sin \phi + 2\omega_e V_n \cos \phi + \frac{V_n V_e}{(N+h) \cos^2 \phi} & 0 & 0 \\ -2\omega_e V_e \cos \phi - \frac{V_e^2}{(N+h) \cos^2 \phi} & 0 & 0 \\ -2\omega_e V_e \sin \phi & 0 & \frac{2g}{M+h} \end{bmatrix} \begin{bmatrix} \delta \phi \\ \delta \lambda \\ \delta h \end{bmatrix} + \begin{bmatrix} -\frac{V_u}{N+h} + \frac{V_n \tan \phi}{N+h} & 2\omega_e \sin \phi + \frac{V_e \tan \phi}{N+h} & -2 \left(\omega_e \cos \phi + \frac{V_e}{N+h} \right) \\ -2 \left(\omega_e \sin \phi + \frac{V_e \tan \phi}{N+h} \right) & -\frac{V_u}{M+h} & -\frac{V_n}{M+h} \\ 2 \left(\omega_e \cos \phi + \frac{V_e}{N+h} \right) & 2 \frac{V_n}{M+h} & 0 \end{bmatrix} \begin{bmatrix} \delta V_e \\ \delta V_n \\ \delta V_u \end{bmatrix} + \begin{bmatrix} 0 & f_u & -f_n \\ -f_u & 0 & f_e \\ f_n & -f_e & 0 \end{bmatrix} \begin{bmatrix} \delta \rho \\ \delta \theta \\ \delta \psi \end{bmatrix} + \mathbf{R}_b^l \begin{bmatrix} \delta f_x \\ \delta f_y \\ \delta f_z \end{bmatrix} \quad (21)$$

In this work the errors in pitch $\delta\rho$ and $\delta\theta$ roll are not modelled inside the KF. This is because they don't suffer from error growth due to lack of integration operations. Therefore there are no dynamic error states for pitch and roll errors. Instead, expressions for $\delta\rho$ and $\delta\theta$ in $\delta\vec{V}^l$ composed of other error states and pitch and roll equations in RISS mechanization are derived. The equation for velocity error is then re-arranged to accommodate the error terms belonging to $\delta\rho$ and $\delta\theta$.

The following is a derivation for the expression for $\delta\rho$ in Equation 21 using Equation 6. Take the derivative of the error component of ρ to give $\delta\rho$:

$$\delta\rho = \left[\frac{d}{df_y} \rho \right] \delta f_y = \left[\frac{d}{df_y} \sin^{-1} \left(\frac{f_y}{g} \right) \right] \delta f_y = \frac{1}{g \sqrt{1 - \left(\frac{f_y}{g} \right)^2}} \delta f_y \quad (22)$$

A similar operation is performed for the error in roll, keeping in mind that the aim is to find an alternate expression for $\delta\theta$ that contains error terms other than $\delta\theta$ and $\delta\rho$. Using Equation 7, the partial derivatives of each component of θ in Equation 21 are used to give:

$$\delta\theta = \left[\frac{\partial}{\partial\theta} \theta \right] \delta\theta = - \left[\frac{\partial}{\partial\theta} \sin^{-1} \left(\frac{f_x + V_f \omega_z}{g \cos \rho} \right) \right] \delta\theta \quad (23)$$

Where $\delta\theta = [\delta V_f \quad \delta\rho \quad \delta\omega_z \quad \delta f_x]^T$. Taking partial derivatives results in:

$$\delta\theta = - \frac{1}{\sqrt{1 - \left(\frac{f_x + V_f \omega_z}{g \cos \rho} \right)^2}} \left(\frac{\omega_z}{g \cos \rho} \delta V_f + \frac{f_x + V_f \omega_z}{g} \left(\frac{\sin \rho}{\cos^2 \rho} \right) \delta\rho + \frac{V_f}{g \cos \rho} \delta\omega_z + \frac{1}{g \cos \rho} \delta f_x \right) \quad (24)$$

Express $\delta\rho$ and its associated terms in Equation 24 using the components from Equation 22 as follows:

$$\begin{aligned} \frac{f_x + V_f \omega_z}{g} \left(\frac{\sin \rho}{\cos^2 \rho} \right) \delta\rho &= \frac{f_x + V_f \omega_z}{g} \left(\frac{\sin \rho}{\cos^2 \rho} \right) \left(\frac{1}{g \sqrt{1 - \left(\frac{f_y}{g} \right)^2}} \delta f_y \right) \\ &= \left(\frac{(f_x + V_f \omega_z) \sin \rho}{g^2 \cos^2 \rho \sqrt{1 - \left(\frac{f_y}{g} \right)^2}} \right) \delta f_y \end{aligned} \quad (25)$$

Express δV_f contained in $\delta\theta$ from Equation 24 in terms of the three velocities along the east, north and up channels:

$$\begin{aligned} \delta V_f &= \left[\frac{\partial}{\partial \vec{V}_f} V_f \right] \delta \vec{V}_f = \left[\frac{\partial}{\partial \vec{V}_f} \sqrt{V_e^2 + V_n^2 + V_u^2} \right] \delta \vec{V}_f \\ &= \frac{1}{\sqrt{V_e^2 + V_n^2 + V_u^2}} [\hat{z} V_e \quad \hat{z} V_n \quad \hat{z} V_u] \begin{bmatrix} \delta V_e \\ \delta V_n \\ \delta V_u \end{bmatrix} = \frac{1}{V_f} [V_e \quad V_n \quad V_u] \begin{bmatrix} \delta V_e \\ \delta V_n \\ \delta V_u \end{bmatrix} \end{aligned} \quad (26)$$

Using Equations 25 and 26, Equation 24 can be rewritten as:

$$\begin{aligned} \delta\theta = & - \left(\frac{\omega_z}{V_f (g \cos \rho) \sqrt{1 - \left(\frac{f_x + V_f \omega_z}{g \cos \rho} \right)^2}} \right) [V_e \ V_n \ V_u] \begin{bmatrix} \delta V_e \\ \delta V_n \\ \delta V_u \end{bmatrix} \\ & - \frac{V_f}{g \cos \rho \sqrt{1 - \left(\frac{f_x + V_f \omega_z}{g \cos \rho} \right)^2}} \delta\omega_z \\ & - \frac{1}{\sqrt{1 - \left(\frac{f_x + V_f \omega_z}{g \cos \rho} \right)^2}} \begin{bmatrix} \frac{1}{g \cos \rho} & \frac{(f_x + V_f \omega_z) \sin \rho}{g^2 \cos^2 \rho \sqrt{1 - \left(\frac{f_y}{g} \right)^2}} \end{bmatrix} \begin{bmatrix} \delta f_x \\ \delta f_y \end{bmatrix} \end{aligned} \quad (27)$$

Using Equations 22 and 27 the equation for the attitude components of the velocity error can be re-arranged to accommodate the error terms belonging to ρ and θ . Similar terms will be grouped to produce a set of equations that describe the attitude errors within $\delta\dot{\vec{V}}^l$. The term $\delta\dot{\vec{V}}_{\text{att}}^l$ will be used to describe the attitude-portion of the velocity errors states. Once the equation for the components of velocity errors due to attitude errors is described it can be easily combined with the other terms in the velocity error states.

$$\begin{aligned} \delta\dot{\vec{V}}_{\text{att}}^l = & \begin{bmatrix} 0 & f_u & -f_n \\ -f_u & 0 & f_e \\ f_n & -f_e & 0 \end{bmatrix} \begin{bmatrix} \delta\rho \\ \delta\theta \\ \delta\psi \end{bmatrix} = \begin{bmatrix} -f_n \\ f_e \\ 0 \end{bmatrix} \delta\psi + \begin{bmatrix} \frac{-f_u V_f}{g \cos \rho \sqrt{1 - \left(\frac{f_x + V_f \omega_z}{g \cos \rho} \right)^2}} \\ 0 \\ \frac{f_e V_f}{g \cos \rho \sqrt{1 - \left(\frac{f_x + V_f \omega_z}{g \cos \rho} \right)^2}} \end{bmatrix} \delta\omega_z \\ & + \begin{bmatrix} \frac{-f_u}{g \cos \rho \sqrt{1 - \left(\frac{f_x + V_f \omega_z}{g \cos \rho} \right)^2}} & \frac{-f_u (f_x + V_f \omega_z) \sin \rho}{g^2 \cos^2 \rho \sqrt{1 - \left(\frac{f_y}{g} \right)^2} \sqrt{1 - \left(\frac{f_x + V_f \omega_z}{g \cos \rho} \right)^2}} \\ 0 & \frac{-f_u}{g \sqrt{1 - \left(\frac{f_y}{g} \right)^2}} \\ \frac{f_e}{g \cos \rho \sqrt{1 - \left(\frac{f_x + V_f \omega_z}{g \cos \rho} \right)^2}} & \frac{f_e (f_x + V_f \omega_z) \sin \rho}{g^2 \cos^2 \rho \sqrt{1 - \left(\frac{f_y}{g} \right)^2} \sqrt{1 - \left(\frac{f_x + V_f \omega_z}{g \cos \rho} \right)^2}} + \frac{f_n}{g \sqrt{1 - \left(\frac{f_y}{g} \right)^2}} \end{bmatrix} \begin{bmatrix} \delta f_x \\ \delta f_y \end{bmatrix} \\ & + \begin{bmatrix} \sqrt{\sigma_{V_f}^2} \\ 0 \\ \sqrt{\sigma_{V_f}^2} \end{bmatrix} W(t) \end{aligned} \quad (28)$$

Experimental data shows that the forward speed originating from the encoders does not suffer from stochastic errors such as stochastic scale factor. This is due to the fact that the robot's

wheels are essentially rigid. Therefore the error in forward speed δV_f contained in $\delta \theta^T$ is expressed as a white noise term using the standard deviation of δV_f . The standard deviation is added to the process noise coupling state vector \mathbf{G} .

2.5.4 Heading error

As mentioned earlier, pitch and roll do not have an error model in this work. This is because errors in pitch and roll do not accumulate as for the other measurements due to a lack of integration operations. To obtain an expression for heading error, use the yaw expression from mechanization for yaw ψ and linearize it by taking the first order terms in the Taylor series expansion. An expression for the error in yaw (and consequently azimuth) is determined:

$$\delta \dot{\psi} = \begin{bmatrix} -\left(\omega_e \cos \phi + \frac{V_e \csc \phi}{R+h}\right) \frac{V_e \tan \phi}{(R+h)^2} \frac{\tan \phi}{R+h} & 1 \end{bmatrix} \begin{bmatrix} \delta \phi \\ \delta h \\ \delta V_e \\ \delta \omega_z \end{bmatrix} \quad (29)$$

2.5.5 Measurement model

Section 2.5.1 described the error-state system model for the KF. The KF also needs a measurement model to be used in the update stage. There are two measurement update models used in this work. The first is when GPS is available and the second is used when there is a GPS outage. During GPS availability both GPS position and velocity are used and the differences between the RISS mechanization position and velocity and those of GPS are used as a measurement. The measurement model is as follows:

$$\bar{z}_k^{GPS} = \mathbf{H}_k^{GPS} \bar{x}_k + \bar{v}_k^{GPS} \quad (30)$$

Where the measurement state vector \bar{z}_k^{GPS} is defined as:

$$\bar{z}_k^{GPS} = \begin{bmatrix} \phi_k^{INS} - \phi_k^{GPS} \\ \lambda_k^{INS} - \lambda_k^{GPS} \\ h_k^{INS} - h_k^{GPS} \\ V_{e_k}^{INS} - V_{e_k}^{GPS} \\ V_{n_k}^{INS} - V_{n_k}^{GPS} \\ V_{u_k}^{INS} - V_{u_k}^{GPS} \\ \omega_{z_k}^{INS} - \omega_{z_k}^{GPS} \end{bmatrix} \quad (31)$$

The design matrix \mathbf{H} is:

$$\mathbf{H}_k^{GPS} = \begin{bmatrix} 1 & 0 & 0 & 0 & 0 & 0 & 0 & 0 & 0 & 0 & 0 & 0 & 0 & 0 \\ 0 & 1 & 0 & 0 & 0 & 0 & 0 & 0 & 0 & 0 & 0 & 0 & 0 & 0 \\ 0 & 0 & 1 & 0 & 0 & 0 & 0 & 0 & 0 & 0 & 0 & 0 & 0 & 0 \\ 0 & 0 & 0 & 1 & 0 & 0 & 0 & 0 & 0 & 0 & 0 & 0 & 0 & 0 \\ 0 & 0 & 0 & 0 & 1 & 0 & 0 & 0 & 0 & 0 & 0 & 0 & 0 & 0 \\ 0 & 0 & 0 & 0 & 0 & 1 & 0 & 0 & 0 & 0 & 0 & 0 & 0 & 0 \end{bmatrix} \quad (32)$$

And \bar{v}_k^{GPS} is a white noise process with zero mean and unity variance. When GPS is not available, forward velocity derived from the wheel encoders together with pitch and azimuth estimates are used as a measurement update. The measurement model is as follows:

$$\bar{z}_k^{odo} = \mathbf{H}_k^{odo} \bar{x}_k + \bar{v}_k^{odo} \quad (33)$$

Where the measurement state vector \bar{z}_k^{odo} is defined as:

$$\bar{z}_k^{odo} = \begin{bmatrix} V_{e_k}^{INS} - V_{e_k}^{odo} \\ V_{n_k}^{INS} - V_{n_k}^{odo} \\ V_{u_k}^{INS} - V_{u_k}^{odo} \end{bmatrix} \quad (34)$$

The design matrix \mathbf{H} is:

$$\mathbf{H}_k^{odo} = \begin{bmatrix} 0 & 0 & 0 & 1 & 0 & 0 & 0 & 0 & 0 & 0 & 0 & 0 & 0 & 0 \\ 0 & 0 & 0 & 0 & 1 & 0 & 0 & 0 & 0 & 0 & 0 & 0 & 0 & 0 \\ 0 & 0 & 0 & 0 & 0 & 1 & 0 & 0 & 0 & 0 & 0 & 0 & 0 & 0 \end{bmatrix} \quad (35)$$

And \bar{v}_k^{odo} is a white noise process having zero mean and unity variance.

3. Experimental setup

3.1 Wheeled mobile robot

Outdoor trajectory tests are conducted to assess the performance of the developed navigation solution; the tests are conducted using a mobile robot shown in fig 2. The robot was developed by a member of NavINST and members of the Electrical and Computer Engineering Department (ECE) at Royal Military College (RMC) of Canada. The mobile robot is three-wheeled and differentially-driven with a quadrature optical encoder coupled to the drive outputs of each motor. Appropriate scaling in the navigation scheme is used to provide angular velocity estimates of each wheel from these encoders. Power on-board the mobile robot comes from three sources, namely (1) two 12V batteries connected to the drive amplifiers and motors, (2) two 12V batteries connected to the sensors and encoder processor board and (3) a battery internal to the laptop mounted on the top level of the robot.

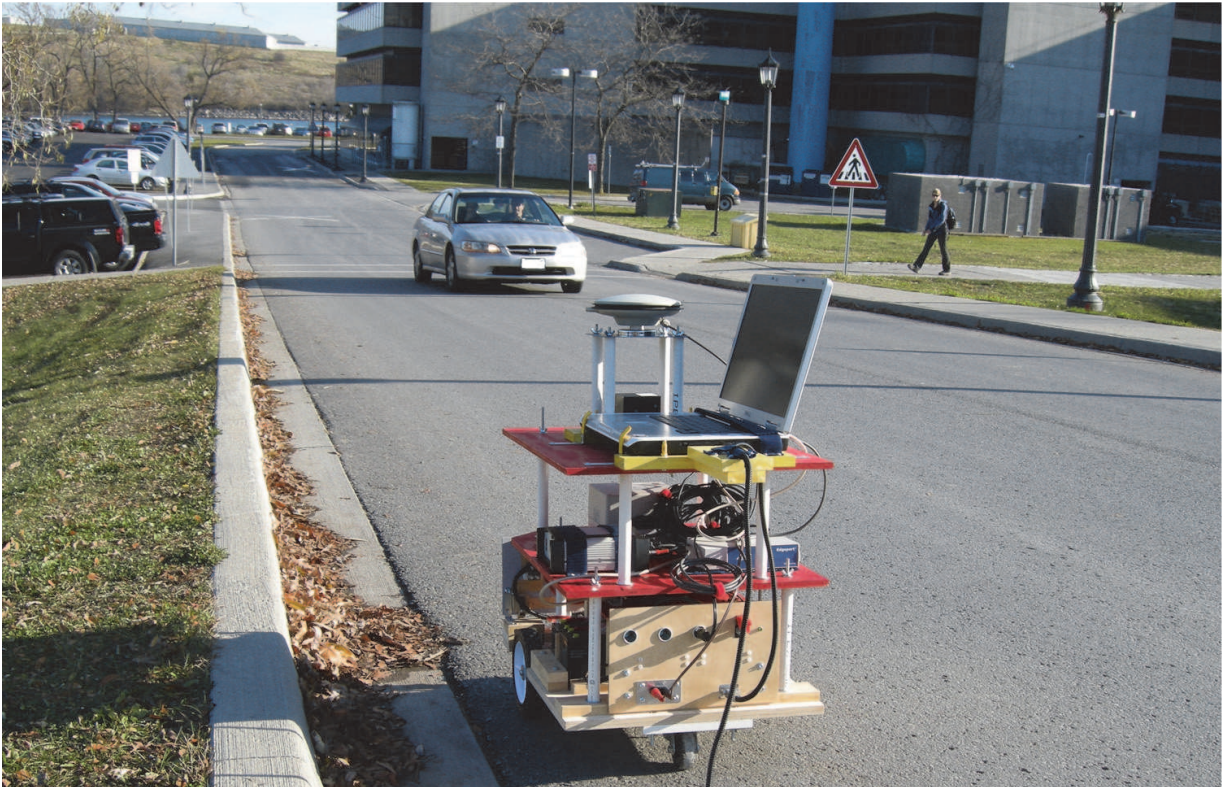


Fig. 2. The mobile robot used for the experiments in this work, custom-built by the author and members of the Electrical and Computer Engineering Department at Royal Military College of Canada.

3.2 Equipment

The inertial sensors used in this work include a MEMS-grade IMU made by Crossbow, model IMU300CC-100. Specifications of this IMU are in table 1 and detailed specifications can be found in (*IMU300CC - 6DOF Inertial Measurement Unit*, 2009). Velocity updates are provided by the forward speed of the robot, derived from encoders coupled to the drive output of each motor. The results of the presented navigation solution are evaluated with respect to a reference solution made by NovAtel where a Honeywell HG1700 high-end tactical grade IMU is integrated with a NovAtel OEM4 GPS receiver. The IMU and GPS receiver are integrated with a G2 Pro-Pack SPAN unit which is an off-the-shelf system developed by NovAtel. The details of this system are described in (*SPAN Technology System User Manual OM-20000062*, 2005). Biases and scale factors for the HG1700 IMU are in table 2 and detailed specification can be found in (*HG1700 Inertial Measurement Unit*, 2009). The high-cost NovAtel SPAN system provides a reference solution to validate the proposed method which uses the low-cost MEMS-based sensors. The SPAN system is also used to examine the overall performance during some GPS outages intentionally introduced in post-processing. A basic block diagram of the sensor electronics on-board the mobile robot appears in fig 3.

4. Results and discussion

Trajectories are carried out using the mobile robot described in Section 3 and sensor data is collected to test the developed solution in post-processing. Four navigation solutions are compared in order to show the benefit of using RISS instead of a full IMU and the benefit of

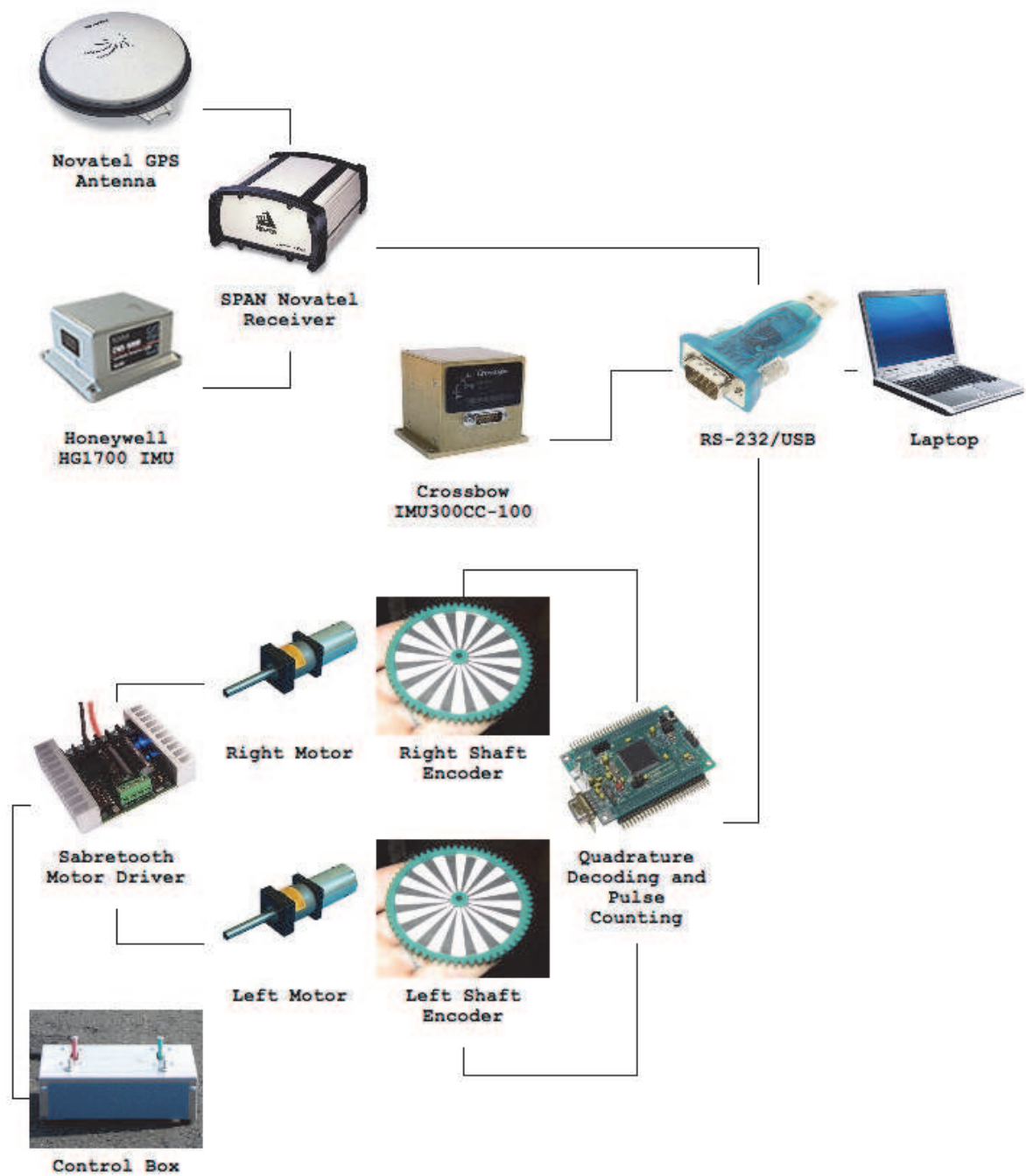


Fig. 3. Block diagram for the electronics on-board the mobile robot used in the experiments.

Crossbow IMU (IMU300CC)			
Gyroscopes		Accelerometers	
Bias, °/sec	< ±2.000	Bias, mg	< ±30.000
Scale Factor, %	< 1.000	Scale Factor, %	1.000
Random Walk, °/√hr	2.250	Random Walk, m/(s√hr)	0.150

Table 1. Bias, scale factor error and random walk for the Crossbow IMU300CC IMU. Adapted from (IMU300CC - 6DOF Inertial Measurement Unit, 2009).

Honeywell IMU (HG1700)			
Gyroscopes		Accelerometers	
Bias, °/hr	1.000	Bias, mg	1.000
Scale Factor, ppm	150.000	Scale Factor, ppm	300.000
Random Walk, °/√hr	0.125		

Table 2. Bias, scale factor error and random walk for the Honeywell HG1700 IMU found in Novatel GPS/INS. Adapted from SPAN Technology System User Manual OM-20000062 (2005) and HG1700 Inertial Measurement Unit (2009).

using velocity updates from wheel encoders during GPS outages. Each of the four navigation solutions are described as follows:

- KF using RISS and velocity updates during GPS outages;
- KF using RISS without updates during outages;
- KF using full IMU with velocity updates during outages; and
- KF using full IMU without updates during outages.

The errors in all the estimated solutions are calculated with respect to the NovAtel reference solution. Results for two trajectories are shown in this work. The first trajectory is shown in fig 4 and is located on-campus at RMC. It forms a loop with start and end at the same position and contains two different sections with hills both at an incline and decline to the robot’s trajectory.

The second trajectory for this experiment is shown in fig 5 and is also located on-campus at RMC. This trajectory forms a loop with start and end at the same position and is much longer than the trajectory in fig 4. It contains several different sections which include hills both at an incline and decline to the robot’s trajectory.

4.1 Trajectory 1

The ultimate check for the proposed system’s accuracy is during GPS signal blockage which can be intentionally introduced in post-processing. Since the presented solution is loosely coupled the outages represent complete blockages of GPS updates. Seven GPS outages are simulated with durations of 60 seconds each. The simulated outages are chosen such that they encompass straight portions, turns, and slopes.

Table 7 shows the root mean square (RMS) error in both the estimated 2-D horizontal position and the estimated altitude during seven GPS outages for the four compared solutions. The

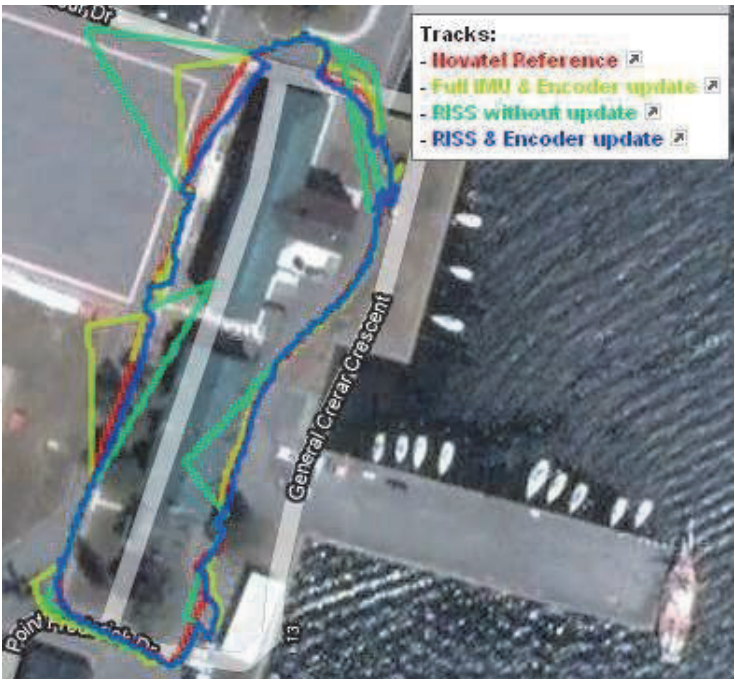


Fig. 6. Three solutions and reference for first trajectory: Red for reference, Yellow for KF using full IMU with velocity updates, Green for KF using RISS without updates, Blue for KF using RISS with velocity updates.

RMS Errors during GPS outages								
Outage No.	1	2	3	4	5	6	7	Average
Duration (s)	60	60	60	60	60	60	60	60
KF full IMU without updates								
h (m)	6.63	25.56	16.30	7.73	17.86	2.26	11.42	12.54
Pos 2D (m)	30.01	26.55	82.14	79.83	37.54	172.52	21.63	64.32
KF full IMU with velocity updates								
h (m)	1.39	13.91	17.22	18.07	1.46	5.38	6.11	9.08
Pos 2D (m)	5.64	1.61	3.32	3.54	7.28	9.10	4.53	5.00
KF RISS without velocity updates								
h (m)	1.20	4.96	9.21	0.27	1.02	0.66	3.86	3.03
Pos 2D (m)	16.43	6.32	2.47	4.07	10.75	21.49	7.21	9.82
KF RISS with velocity updates								
h (m)	1.43	0.68	3.61	0.44	0.43	1.38	1.86	1.40
Pos 2D (m)	2.48	1.21	2.96	0.76	2.39	3.05	1.60	2.06

Fig. 7. RMS errors for altitude and 2D position for the seven outages in first trajectory.

The benefit of using wheel encoders to provide velocity updates during GPS outages can be seen by two comparisons. The first comparison uses KF with full IMU and considers two sets of results, one with and the second without velocity updates. With velocity updates the solution has an average of the maximum positional error for the seven GPS outages equal to 8.77 meters while the case without updates has 139.3 meters of error. The second comparison uses KF with RISS and considers two sets of results, one with and the second without velocity updates. With velocity updates the solution has an average of the maximum positional error for the seven GPS outages equal to 3.35 meters while the case without updates has 18.67 meters of error.

Max Errors during GPS outages								
Outage No.	1	2	3	4	5	6	7	Average
Duration (s)	60	60	60	60	60	60	60	60
KF full IMU without updates								
h (m)	9.76	46.81	27.02	11.91	34.49	5.02	21.24	22.32
Pos 2D (m)	64.22	55.19	183.07	163.18	96.39	366.10	46.85	139.29
KF full IMU with velocity updates								
h (m)	4.96	24.31	29.16	28.15	1.69	8.97	9.46	15.24
Pos 2D (m)	8.98	2.00	5.62	7.44	13.23	17.00	7.15	8.77
KF RISS without velocity updates								
h (m)	4.97	9.46	13.36	0.61	2.17	1.84	4.72	5.30
Pos 2D (m)	34.42	12.40	4.83	9.26	17.88	38.39	13.51	18.67
KF RISS with velocity updates								
h (m)	3.51	2.83	3.75	0.58	0.82	1.71	2.04	2.18
Pos 2D (m)	3.36	1.99	5.91	1.23	3.21	4.79	2.97	3.35

Fig. 8. Maximum errors for altitude and 2D position for the seven outages in first trajectory.

When comparing KF with RISS and velocity updates to KF with full IMU and velocity updates the advantage of RISS can be clearly noticed. The former has an average of the maximum positional error for the seven GPS outages equal to 3.35 meters while the latter shows an error of 8.77 meters.

These results together with the trajectory plots in fig 6 demonstrate that the proposed 3-D localization solution using KF for RISS/GPS integration and employing velocity updates using wheel encoders outperforms all the other compared solutions. Furthermore this solution provides very good results when compared to the MEMS-based INS/GPS integration results in the literature.

4.2 Trajectory 2

The second trajectory is much longer than the first one and enables the examination of long GPS outages. Seven outages are simulated with the duration of each outage equal to 150 seconds. This duration is chosen to test the performance of the proposed navigation solution in long GPS outages. The simulated outages are also chosen such that they encompass straight portions, turns and slopes.

Table 10 shows the root mean square (RMS) error in both the estimated 2-D horizontal position and the estimated altitude during the seven GPS outages for the four compared solutions. Table 11 shows the maximum errors in the estimated 2-D horizontal position and the estimated altitude during each outage. fig 9 shows a 2-D plot of four tracks, namely: (1) reference solution, (2) KF with full IMU and velocity updates during GPS outages, (3) KF with RISS and without updates during outages and (4) KF with RISS and velocity updates during outages. As mentioned earlier the KF with full IMU and without updates during GPS outages is not shown because the position errors would dramatically change the scale of the plot and make comparison of the other solutions very difficult.

The results in table 10 and table 11 confirm the results of the first trajectory and they further demonstrate the advantage of RISS over a full IMU. One can see a great difference in 2-D positional errors when comparing the results of KF with full IMU without updates with the results of KF with RISS without updates during during GPS outages. While the former technique has an average of the maximum positional error for the seven GPS outages equal to

789.2 meters the latter shows an error of 68.29 meters. The reason for this huge enhancement of performance is the use of accelerometers vice the two gyroscopes used to get pitch and roll from the RISS.

As seen in the first trajectory the benefit of using velocity updates during GPS outages derived from the wheel encoders is seen by two comparisons. The first comparison uses KF with full IMU and considers two sets of results, one with and the second without velocity updates. With velocity updates the solution has an average of the maximum positional error for the seven GPS outages equal to 11.44 meters while the case without updates has 789.2 meters of error.



Fig. 9. Three solutions and reference for second trajectory: Red for reference, Yellow for KF using full IMU with velocity updates, Green for KF using RISS without updates, Blue for KF using RISS with velocity updates.

RMS Errors during GPS outages								
Outage No.	1	2	3	4	5	6	7	Average
Duration (s)	150	150	150	150	150	150	150	150
KF full IMU without updates								
h (m)	118.33	7.4394	70.7598	33.7392	49.571	138.992	393.058	115.98
Pos 2D (m)	224.16	395.08	474.40	155.13	209.99	654.03	308.26	345.86
KF full IMU with velocity updates								
h (m)	4.52	4.24	6.78	8.05	15.85	11.48	29.22	11.45
Pos 2D (m)	6.8248	3.8805	7.6824	3.4269	2.5439	13.9607	9.0778	6.771
KF RISS without velocity updates								
h (m)	32.44	19.20	20.55	33.36	50.89	24.52	50.80	33.11
Pos 2D (m)	39.03	22.72	48.03	55.68	57.21	27.28	52.12	43.15
KF RISS with velocity updates								
h (m)	2.86	2.39	2.33	3.18	2.09	4.52	3.86	3.03
Pos 2D (m)	4.35	9.58	5.71	4.26	0.85	1.04	7.41	4.74

Fig. 10. RMS errors for altitude and 2D position for the seven outages in second trajectory.

The second comparison uses KF with RISS and considers two sets of results, one with and the second without velocity updates. With velocity updates the solution has an average of

Max Errors during GPS outages								
Outage No.	1	2	3	4	5	6	7	Average
Duration (s)	150	150	150	150	150	150	150	150
KF full IMU without updates								
h (m)	261.20	10.21	145.67	60.44	106.94	314.92	897.83	256.75
Pos 2D (m)	528.2	874.4	1069.2	294.7	466.8	1601.6	689.5	789.2
KF full IMU with velocity updates								
h (m)	6.40	6.93	11.50	16.71	22.81	21.63	50.73	19.53
Pos 2D (m)	10.11	6.46	10.92	6.37	5.19	22.61	18.43	11.44
KF RISS without velocity updates								
h (m)	47.20	31.74	89.46	83.49	53.21	31.73	18.87	50.81
Pos 2D (m)	72.67	41.55	45.74	70.76	112.95	49.31	85.07	68.29
KF RISS with velocity updates								
h (m)	3.33	2.78	2.75	3.47	4.16	5.06	4.2	3.68
Pos 2D (m)	6.92	16.32	9.52	6.68	1.24	1.31	11.52	7.64

Fig. 11. Maximum errors for altitude and 2D position for the seven outages in second trajectory.

the maximum positional error for the seven GPS outages equal to 7.64 meters while the case without updates has 68.29 meters of error.

When comparing KF with RISS and velocity updates to KF with full IMU and velocity updates the advantage of RISS can be seen especially in the altitude component. The former has an average of the maximum positional error for the seven GPS outages equal to 7.64 meters while the latter shows an error of 11.44 meters. The former has an average of the maximum altitude error for the seven GPS outages equal to 3.68 meters while the latter shows an error of 19.53 meters.

These results together demonstrate that the 3-D localization solution using KF for RISS/GPS integration and employing velocity updates using wheel encoders outperforms all the other compared solutions. Furthermore this solution provides very good results when compared to the MEMS-based INS/GPS integration results in the literature.

5. Conclusion and future work

This chapter presented an outdoor 3-D localization solution for mobile robots using low-cost MEMS-based sensors, wheel encoders and GPS. A reduced inertial sensor system was used for both decreasing the cost and improving the performance. The integration was achieved using a loosely-coupled KF. In this work, a predictive error model for KF was developed for estimating the errors in positions, velocities and attitude provided by RISS mechanization. Using this error model inside the KF gives good results during GPS outages that outperformed the full IMU results. Furthermore, when this KF is used with measurement updates using forward velocity from encoders together with pitch and azimuth estimates (during GPS outages) it provides better results and outperforms all the compared solutions.

The positioning solutions in this work were tested with two real trajectories with seven simulated GPS outages whose duration was 60 seconds in the first trajectory and 150 seconds in the second trajectory. The proposed solutions were discussed and compared with each solution also compared against a reference solution. Considering the maximum error in horizontal positioning in the first trajectory, the KF with RISS and velocity updates during GPS outages achieved an average improvement of approximately 97.6% over KF with full IMU without any updates during outages, of approximately 61.8% over KF with full IMU

with velocity updates during outages, and of approximately 82.0% over KF with RISS without any updates during outages. Considering the maximum error in horizontal positioning in the first trajectory, the KF with RISS and velocity updates during GPS outages achieved an average improvement of approximately 99.0% over KF with full IMU without any updates during outages, of approximately 33.2% over KF with full IMU with velocity updates during outages, and of approximately 88.8% over KF with RISS without any updates during outages. These results show the superiority of the proposed localization solution.

One problem unique to small wheeled robots with strap-down navigation systems is that there is a great deal of chassis rigidity that passes along any disturbances felt at the wheels of the robot. Small, low-cost robots do not have suspension systems found on full-size vehicles which prevent many disturbances from being measured by the accelerometers of a strap-down IMU. A future investigation is required regarding low-cost measures for dampening some of the vibrations caused by small obstacles and imperfections on the road surface. Prospective researchers should make a careful selection of tires for their small mobile robot that allow moderate deformation to small obstacles while preserving sufficient shape to maintain reliable estimates for velocities measured by the wheel encoders.

Kalman filtering is a good technique for reducing the stochastic error of a system since it requires little processing time compared to other algorithms. It is a suitable choice for deployment in low-cost, low-power, low-form-factor systems such as those found on small mobile robots. Further study is required to determine the performance of the techniques outlined in this work in the context of an embedded system operating in real-time.

6. Acknowledgements

To our family and friends for their love, support and commitment. This chapter wouldn't have been possible without them.

7. References

- Borenstein, J., Everett, H., Feng, L. & Wehe, D. (1997). Mobile robot positioning: Sensors and techniques, *Journal of Robotic Systems* 14(4): 231–249.
- Chong, K. S. & Kleeman, L. (1997). Accurate odometry and error modelling for a mobile robot, *Proceedings of the 1997 IEEE International Conference on Robotics and Automation*, Vol. 4, Albuquerque, NM, pp. 2783–2788.
- Cox, I. J. (1991). Blanche - an experiment in guidance and navigation of an autonomous robot vehicle, *IEEE Transactions on Robotics and Automation* 7(2): 193–204.
- Farrell, J. A. & Barth, M. (1998). *The Global Positioning System & Inertial Navigation*, McGraw-Hill.
- Grewal, M. S., Weill, L. R. & Andrews, A. P. (2007). *Global Positioning Systems, Inertial Navigation, and Integration*, John Wiley and Sons.
- HG1700 Inertial Measurement Unit (2009).
URL: http://www51.honeywell.com/aero/common/documents/myaerospacecatalog-documents/Missiles-Munitions/HG1700_Inertial_Measurement_Unit.pdf
- IMU300CC - 6DOF Inertial Measurement Unit (2009).
URL: www.xbow.com/Products/Product_pdf_files/Inertial_pdf/IMU300CC_Datasheet.pdf

- Iqbal, U., Karamat, T. B., Okou, A. F. & Noureldin, A. (2009). Experimental results on an integrated gps and multi sensor system for land vehicle positioning, *International Journal of Navigation and Observation* 2009.
- Iqbal, U., Okou, A. F. & Noureldin, A. (2008). An integrated reduced inertial sensor system - riss/gps for land vehicle, *IEEE/ION Position, Location and Navigation Symposium (PLANS) 2008*, Monterey, California, USA, pp. 912–922.
- Noureldin, A., Irvine-Halliday, D. & Mintchev, M. P. (2002). Accuracy limitations of fog-based continuous measurement-while-drilling surveying instruments for horizontal wells, *IEEE Transactions on Instrumentation and Measurement* 51(6): 1177–1191.
- Noureldin, A., Irvine-Halliday, D. & Mintchev, M. P. (2004). Measurement-while-drilling surveying of highly-inclined and horizontal well sections utilizing single-axis gyro sensing system, *Measurement Science and Technology* 15(12): 2426–2434.
- Noureldin, A., Karamat, T., Eberts, M. D. & El-Shafie, A. (2009). Performance enhancement of mems based ins/gps integration for low cost navigation applications, *IEEE Transactions on Vehicular Technology* 58(3): 1077–1096.
- Ohno, K., Tsubouchi, T., Shigematsu, B., Maeyama, S. & Yuta, S. (2003). Outdoor navigation of a mobile robot between buildings based on DGPS and odometry data fusion, *Proceedings of the IEEE International Conference on Robotics and Automation*, Vol. 2, IEEE Press, pp. 1978–1984.
- Ollero, A., Arrue, B. C., Ferruz, J., Heredia, G., Cuesta, F., López-Pichaco, F. & Nogales, C. (1999). Control and perception components for autonomous vehicle guidance. application to the romeo vehicles, *Control Engineering Practice* 7(10): 1291–1299.
- Pacis, E., Everett, H., Farrington, N. & Bruemmer, D. (2004). Enhancing functionality and autonomy in man-portable robots, *SPIE Proc. 5804: Unmanned Ground Vehicle Technology VII*, Orlando, FL, USA.
- Pacis, E., Everett, H., Farrington, N., Kogut, G., Sights, B., Kramer, T., Thompson, M., Bruemmer, D. & Few, D. (2005). Transitioning unmanned ground vehicle research technologies, *SPIE Proceedings 5804: Unmanned Ground Vehicle Technology VII*, Orlando, FL, USA.
- SPAN Technology System User Manual OM-20000062 (2005).
URL: www.novatel.com/Documents/Manuals/om-20000062.pdf

IntechOpen



Global Navigation Satellite Systems: Signal, Theory and Applications

Edited by Prof. Shuanggen Jin

ISBN 978-953-307-843-4

Hard cover, 426 pages

Publisher InTech

Published online 03, February, 2012

Published in print edition February, 2012

Global Navigation Satellite System (GNSS) plays a key role in high precision navigation, positioning, timing, and scientific questions related to precise positioning. This is a highly precise, continuous, all-weather, and real-time technique. The book is devoted to presenting recent results and developments in GNSS theory, system, signal, receiver, method, and errors sources, such as multipath effects and atmospheric delays. Furthermore, varied GNSS applications are demonstrated and evaluated in hybrid positioning, multi-sensor integration, height system, Network Real Time Kinematic (NRTK), wheeled robots, and status and engineering surveying. This book provides a good reference for GNSS designers, engineers, and scientists, as well as the user market.

How to reference

In order to correctly reference this scholarly work, feel free to copy and paste the following:

Eric North, Jacques Georgy, Umar Iqbal, Mohammed Tarbochi and Aboelmagd Noureldin (2012). Improved Inertial/Odometry/GPS Positioning of Wheeled Robots Even in GPS-Denied Environments, Global Navigation Satellite Systems: Signal, Theory and Applications, Prof. Shuanggen Jin (Ed.), ISBN: 978-953-307-843-4, InTech, Available from: <http://www.intechopen.com/books/global-navigation-satellite-systems-signal-theory-and-applications/improved-inertial-odometry-gps-positioning-of-wheeled-robots-even-in-gps-denied-environments>

INTECH
open science | open minds

InTech Europe

University Campus STeP Ri
Slavka Krautzeka 83/A
51000 Rijeka, Croatia
Phone: +385 (51) 770 447
Fax: +385 (51) 686 166
www.intechopen.com

InTech China

Unit 405, Office Block, Hotel Equatorial Shanghai
No.65, Yan An Road (West), Shanghai, 200040, China
中国上海市延安西路65号上海国际贵都大饭店办公楼405单元
Phone: +86-21-62489820
Fax: +86-21-62489821

© 2012 The Author(s). Licensee IntechOpen. This is an open access article distributed under the terms of the [Creative Commons Attribution 3.0 License](https://creativecommons.org/licenses/by/3.0/), which permits unrestricted use, distribution, and reproduction in any medium, provided the original work is properly cited.

IntechOpen

IntechOpen